Spin-vibration interaction in a nanomechanical spin-valve

P. Stadler,[1] W. Belzig,[1] and G. Rastelli[1,2]

[1] *Fachbereich Physik, Universität Konstanz, D-78457 Konstanz, Germany*
[2] *Zukunftskolleg, Fachbereich Physik, Universität Konstanz, D-78457, Konstanz, Germany*

(Dated: August 28, 2014)

We study spin-dependent transport in a suspended carbon nanotube quantum dot in contact with two ferromagnetic leads and with the dot's spin coupled to the flexural modes. We consider a spin-vibrational interaction inducing spin-flip processes between the two Zeeman levels of the dot due to spin-orbit interaction or a magnetic field gradient. The inelastic vibration-assisted spin-flips give rise to a mechanical damping and for an applied bias-voltage to a steady non-equilibrium occupation of the harmonic oscillator. We discuss how these effects depend on the Zeeman splitting and the magnetic polarization of the leads. Depending on the magnetic configuration and the bias voltage polarity, the vibration can be cooled or become unstable. Owing to the sensitivity of the electron transport to the spin orientation, we find signatures of the nanomechanical motion in the current-voltage characteristic even for weak spin-vibrational coupling. Hence, the vibrational state can be read out in the current-voltage characteristic.

PACS numbers: 73.63.-b,71.38.-k,85.85.+j,75.76.+j

I. INTRODUCTION

Advances in the fabrication of nanoelectromechanical systems (NEMS)[1,2] have open the possibility to measure extremely small forces and masses.[3,4]As the displacements of mechanical vibrations are conveniently registered by the electron transport measurements, NEMS may prove also useful technologically as ultra-sensitive detectors of charge[5] and spin.[6] High-frequency NEMS devices operating at cryogenic temperatures can themselves approach the full quantum regime and pave the way for testing quantum mechanics in solid-objects formed by a macroscopic number of atoms.[7–9] Recent experiments realized the quantum ground state in different type of nanomechanical resonators.[10–12] Despite this variety, a common and promising strategy for the achievement of the quantum mechanical regime consists in interfacing the mechanical degree of freedom with an elemental quantum object, i.e. a quantum two-level system such as superconducting Josephson qubits[13], single Andreev levels[14] or single spins.[15,16] Successful accomplishment of this strategy was reported for a nanomechanical dilatation resonator coupled to a phase-qubit.[17] This experiment and others motivate the interest in hybrid quantum nano-systems containing nanomechanical oscillators approaching their quantum regime.[18,19]

Concerning the spin-oscillator systems, a variety of nanomechanical devices have been proposed. For instance, systems consisting of mechanical cantilevers with a ferromagnetic tip coupled to magnetic moments of a solid sample have been extensively studied in the context of Magnetic Resonance Force Microscopy (MRFM).[6,20–22] In this case, the interaction between the nanomechanical resonator and the spin arises from the relative motion of the spin in the inhomogeneous magnetic field created by the tip. In the MRFM-experiments, realized at room or low-temperature, the ultimate goal was the mechanical detection, spatially resolved, of a single electron spin[6] or thousands of nuclear spins with nanometer resolution.[21] In another series of experiments, the spin was exploited for sensing the motion of the mechanical resonator, i.e. magnetized micro-cantilevers coupled to the magnetic spin associated to a nitrogen-vacancy (NV) center in diamond.[23,24] In both cases, the state of the spin or the oscillator's position (MRFM-scheme) were probed via optical measurements.

The interplay between mechanical motion and spin-transport has been also discussed for nanomechanical torsion oscillators at the interface between a ferromagnetic and nonmagnetic conductors.[25,26] In this configuration the main operating principle is the spin-flip torsional balance: a change of angular momentum (spin-flip) creates a torque in similarly way to the Einstein-de Haas effect[27] which can be detected in the torsion oscillator. Experimental detection of the mechanical torque induced by the itinerant spins was reported in such devices.[28]

A microscopic realization of similar ideas was accomplished in a recent experiment of Ref. 29, in which the magnetization reversal (spin-flip) of a single molecule magnet grafted to a suspended carbon nanotube (CNT) was probed through electrical transport measurements. Resonant incoherent relaxation between two magnetic states was observed and related to the resonant spin-vibration coupling between the single magnet and a single vibrational mode of the suspended carbon nanotube.

Suspended carbon nanotube quantum dots (CNTQDs) have been also discussed as a suitable playground for the realization of a coherent quantum spin-vibration system.[30–40] In such a case, the spin of the discrete dot's electron levels, formed on the CNT, are coupled to the vibration. An extrinsic mechanism of coupling was proposed in Ref. 41 between the electron spin and the flexural modes of a suspended CNTQD under a magnetic field. On the other hand, the spin-orbit interaction[42,43] in CNTQD provides an intrinsic way to couple the electron spin and the flexural vibration[44,45] (a similar mechanism

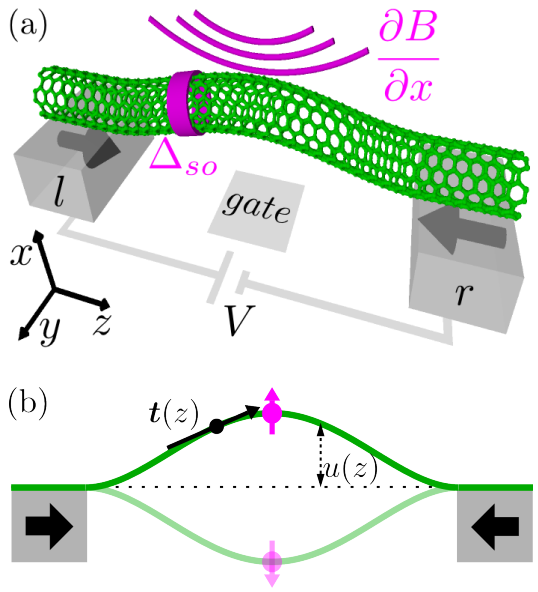

Figure 1. Schematic views of a carbon nanotube quantum dot suspended between two ferromagnetic leads. (a) The spin-vibration interaction can be either induced by the intrinsic spin-orbit coupling Δ_{SO} or by a magnetic gradient $\partial B/\partial x$. (b) Due to the spin-vibration interaction, the dot spin's component $\hat{\sigma}_x$ parallel to the mechanical displacement u couples to the flexural mode. The local tangent vector is denoted by $\boldsymbol{t}(z)$.

was theoretically discussed between spin and phonons in quantum dots in semiconductor heterostructures, see Ref. 46). In qualitative picture, this microscopic interaction acts as an effective magnetic gradient seen by the spin, which is modulated by the mechanical motion,[44] in a similar way as in the MRFM setup.[6,20] This spin-orbit interaction in suspend CNTQDs was theoretically discussed for the realization of a qubit in a single mode cavity.[44] In another recent study, this interaction was employed for the detection of the vibrational motion in a Pauli-spin-Blockade setup using two CNTQDs in series.[45,47]

Motivated by the growing interest in spin-vibration coupling and spin-transport, in this work we discuss the effects of the spin-vibration interaction when the suspended CNTQD is sandwiched between two ferromagnets and a bias-voltage is applied. Such a system acts as nanomechanical spin-valve. Indeed, spin-current injection has been experimentally reported in CNTs in spin-valve geometry.[48–50] As compared to other spin-valve systems, CNTQD offers also the possibility of the gate-field control in the quantum dot regime.[49–51]

We consider a model with a single mechanical model of frequency ω. In the first part, we calculate the mechanical damping and the nonequilibrium occupation n of the harmonic oscillator determined by the electron current flowing through the dot. In comparison to our previous work [52], we show the results for the regimes in which: i) a mechanical instability occurs (negative damping coefficient) , ii) a single lead is polarized. In the second part, we study the effect of the spin-vibration interaction on the current. In particular, we show that remarkable features appear in the current-voltage characteristic when the oscillator is driven in a non-equilibrated state (active cooling and heating).

The paper is structured as follows. In Sec. II, we introduce the model-Hamiltonian and report the results for the steady-state nonequilibrium phonon occupation and the current calculated using the Keldysh nonequilibrium Greens functions approach (NEGF) to the first leading order in the spin-vibrational coupling. In Sec. III, we discuss the nonequilibrium phonon occupation and focus on two aspects: the mechanical instability (negative total damping coefficient) of the resonator and a single polarized lead. The signatures of the spin-vibration interaction in the current are studied in Sec. IV. In the Sec. V we summarize our work.

II. MODEL AND APPROXIMATION

A. Microscopic derivation of the Hamiltonian

The nanomechanical spin-valve that we consider consists of a suspended CNTQD in contact with ferromagnetic leads [Fig. 1]. In this section, we introduce the Hamiltonian of the CNTQD and derive the spin-vibration interaction induced by the spin-orbit coupling or by the application of a magnetic gradient.

1. *Carbon nanotube quantum dot*

In a confining potential, each localized electronic level of the CNTQD is fourfold degenerate owing to the spin- and orbital degree of freedom[53]. We denote the corresponding states as $|\tau,\sigma\rangle$ with $\tau=\pm$ and $\sigma=\pm$ referring to orbital- and spin states, respectively. We chose the spin-quantization axis along the z-direction. The effective low-energy Hamiltonian is given by[44,45,54,55]

$$\hat{H}_{cnt}=\frac{\Delta_{SO}}{2}\tau_3\mathbf{t}(z)\cdot\hat{\boldsymbol{\sigma}}-\mu_{orb}\hat{\tau}_3\mathbf{B}\cdot\mathbf{t}(z)+\mu_B\mathbf{B}\cdot\hat{\boldsymbol{\sigma}}+\Delta_{KK'}\hat{\tau}_1\,, \tag{1}$$

with the orbital magnetic moment μ_{orb} and the Bohr magneton μ_B, the intrinsic spin-orbit coupling Δ_{SO}, the coupling $\Delta_{KK'}$ between different orbital states due to disorder and a magnetic field $\boldsymbol{B}$. The Pauli matrices in spin (orbital) space are denoted as $\hat{\boldsymbol{\sigma}}=(\hat{\sigma}_x,\hat{\sigma}_y,\hat{\sigma}_z)$ ($\hat{\boldsymbol{\tau}}=(\hat{\tau}_1,\hat{\tau}_2,\hat{\tau}_3)$) and the local tangent vector at each point of the tube is written as $\mathbf{t}(z)$ whose direction varies with position z [Fig. 1(b)]. Since typically $\Delta_{KK'}\ll(\Delta_{SO},\mu_{orb}B,\mu_BB)$, we neglect the coupling between different orbitals in the following as we discuss transport far away from the regime in which the energy crossing point between different orbitals occurs.

The deflection associated with the flexural mode leads to a coupling of the spin on the quantum dot with the vibration which is either mediated by the spin-orbit coupling or by a magnetic gradient. The electronic model and the coupling induced by the spin-orbit coupling was studied in Refs. 44, 45 and 47. Here, we additionally derive the coupling between the deflection and the spin due to a magnetic gradient. This coupling arises from the relative motion of the suspended nanotube in a magnetic gradient added to the homogeneous magnetic field B.[56].

We refer to Fig. 1 for the choice of the orientation axis and we assume that the nanotube oscillates in the x-z plane. The deflection $\hat{u}(z)$ can be written in terms of creation and annihilation operators as $\hat{u}(z) = \sum_n f_n(z) u_n (\hat{b}_n + \hat{b}_n^\dagger)$ with the waveform $f_n(z)$ and the zero-point amplitude u_n. For a suspended elastic rod with sufficient strong tension, the waveform is given by $f_n(z) = \sqrt{2}\sin[\pi(n+1)z/L]$ for integers $n \geq 0$ with the eigenfrequency $\omega_n = (n+1)\,\pi\sqrt{T/(\rho L^2)}$, length L and density ρ.[52] If the deflections are small, we can write the variation of the tangent vector as $\delta\mathbf{t}(z) \simeq (d\hat{u}(z)/dz, 0, 0)$. Additionally, the magnetic field at the location of the spin changes by $\delta\mathbf{B} = (\partial\mathbf{B}/\partial x)\hat{u}(z)$ due to the magnetic gradient. We then can expand $\mathbf{B}\cdot\mathbf{t}(z) \simeq B_z + \mathbf{B}\cdot\delta\mathbf{t}(z) + \delta\mathbf{B}\cdot\hat{z}$ in which we neglect $\delta\mathbf{t}(z)\cdot\delta\mathbf{B}$ corresponding to higher-order terms in $\hat{u}$ ($\hat{z}$ denotes the unit vector in z-direction). In the following, we assume a leading magnetic gradient dB_x/dx perpendicular to the nanotube z-axis and neglected the variation of the y- and z-component of the magnetic field along the x-axis $dB_{y,z}/dx = 0$. Furthermore, we assume a vanishing magnetic field in x-direction $B_x = 0$. Inserting the expansion of $\boldsymbol{B}$ and $\boldsymbol{t}(z)$ into Eq. (1) and projecting the Hamiltonian on a flexural mode f_n in the z-axis we obtain[44,52]

$$\hat{H}_{cnt} = \hat{\tau}_3\left(\frac{\Delta_{SO}}{2}\hat{\sigma}_z - \mu_{orb}B_z\right) + \mu_B B_z\hat{\sigma}_z + \hat{H}_{SV,1} + \hat{H}_{SV,2}\,, \tag{2}$$

with

$$\hat{H}_{SV,1} = \mu_B\frac{\partial B_x}{\partial x}\langle f_n(z)\rangle\, u_n\left(\hat{b}_n + \hat{b}_n^\dagger\right)\hat{\sigma}_x \tag{3}$$

$$\hat{H}_{SV,2} = \frac{\Delta_{SO}}{2}\langle f_n'(z)\rangle u_n\left(\hat{b}_n + \hat{b}_n^\dagger\right)\hat{\tau}_3\hat{\sigma}_x\,, \tag{4}$$

in which the waveform f_n is averaged over the electronic orbital in the dot (we also assumed that the variation of the gradient along the nanotube axis is negligible). For a quantum dot formed with symmetric orbital electronic density, the coupling elements $\langle f_n(z)\rangle$ ($\langle f_n'(z)\rangle$) vanish for all odd (even) harmonics. To give a simple estimation, we consider a uniform distribution of the electronic charge on the dot and we obtained $\langle f_0(z)\rangle = 2\sqrt{2}/\pi$ for the first even mode (fundamental) and $\langle df_1(z)/dz\rangle = 2\sqrt{2}/L$ for the first odd mode. In this way, coupling constant $\lambda_n \simeq \mu_B(\partial B_x/\partial x)u_n\langle f_n(z)\rangle$ of $\hat{H}_{SV,1}$ can be estimated by $\lambda = 0.5$ MHz for the fundamental (even) mode with $\partial B_x/\partial x = 5\cdot 10^6$ T/m[22]. The coupling constant $\lambda_n \simeq (\Delta_{SO}/2)u_n\langle df_n(z)/dz\rangle$ in $\hat{H}_{SV,2}$ is estimated to $\lambda \sim 2.5$ MHz for the first odd mode with $\Delta_{SO} \simeq 400$ μeV.[44]

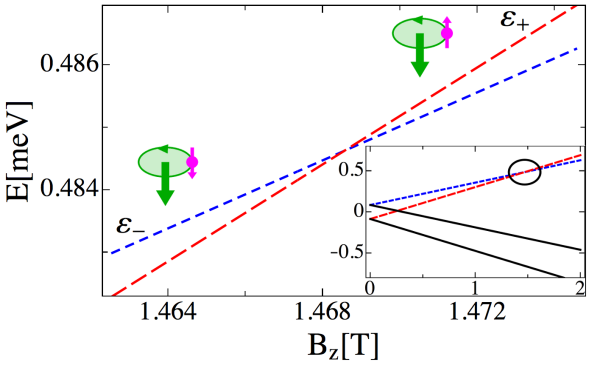

Figure 2. (Colors online) Spectrum of the Hamiltonian for a defect-free carbon nanotube quantum dot. The inset shows the full spectrum as a function of the magnetic field along the nanotube axis. Our model is restricted to the eigenvalues ε_+ and ε_- corresponding to equivalent orbital and opposite spin momentum. The sketches illustrate the direction of the orbital (large green arrow) and spin (small magenta arrow) magnetic moments along the z-axis. The parameters are taken from Ref. [57].

2. *Nanomechanical spin-valve*

The CNTQD is embedded between ferromagnetic leads. We model the two ferromagnets with the Stoner model in which one assumes a strong spin asymmetry in the density of states for the spin-up and down density $\rho_{\alpha\sigma} = \rho_\alpha(1+\sigma p_\alpha)$ with the degree of spin polarization in the $\alpha-$lead defined as $p_\alpha = (\rho_{\alpha+} - \rho_{\alpha-})/(\rho_{\alpha+} + \rho_{\alpha-})$. The effect of the ferromagnets is captured by the spin-dependent tunneling rates $\Gamma_\alpha^\sigma = \pi|t_{\alpha\sigma}|^2\rho_{\alpha\sigma}$. The full Hamiltonian of the spin-valve is given by

$$\hat{H} = \hat{H}_l + \hat{H}_t + \hat{H}_d\,, \tag{5}$$

where the Hamiltonian for the leads ($\alpha = L, R$) reads $\hat{H}_l = \sum_{\alpha\sigma k}\varepsilon_{k\sigma}\hat{c}_{\alpha k\sigma}^\dagger\hat{c}_{\alpha k\sigma}$ and the tunneling Hamiltonian is $\hat{H}_t = \sum_{\alpha\sigma k}(t_{\alpha\sigma}\hat{c}_{\alpha k\sigma}^\dagger\hat{d}_\sigma + h.c.)$. The operators $\hat{c}_{\alpha k\sigma}^\dagger$ ($\hat{c}_{\alpha k\sigma}$) and $\hat{d}^\dagger$ ($\hat{d}$) are creation (annihilation) operators for the corresponding electronic states in the ferromagnetic leads and the dot states. We restrict our discussion to a part of the spectrum of the CNTQD, i.e. the situation in which only two spin-channels for the same orbital level are involved in the relevant range as shown in Fig. 2. This regime occurs when the orbital-energy splitting is the largest energy-scale in the Hamiltonian (1). The model Hamiltonian capturing the two spin state of the same valley, the spin-vibration interaction and a single

mechanical mode is given by

$$\hat{H}_d = \sum_\sigma \varepsilon_\sigma \hat{d}^\dagger_\sigma \hat{d}_\sigma + \lambda \hat{\sigma}_x \left(\hat{b}^\dagger + \hat{b}\right) + \hbar\omega \hat{b}^\dagger \hat{b}\,, \qquad (6)$$

with the energy level of the dot and the splitting between the two spin-state given by $\varepsilon_\sigma = \varepsilon_0 + \sigma\varepsilon_z/2$. The $x-$component of the local spin operator in the dot $\hat{\sigma}_x = \hat{d}^\dagger_+ \hat{d}_- + \hat{d}^\dagger_- \hat{d}_+$ is chosen to be perpendicular to the quantization axis for the spin transport. The bosonic operators are denoted as $\hat{b}$ and $\hat{b}^\dagger$ and we model the oscillator as a single mode with frequency ω.

The Hamiltonian Eq. (6) is similar to the well-known Anderson-Holstein model widely discussed in literature[58–71] in which the quantum oscillator is linearly coupled to the dot charge $\hat{n} = \hat{d}^\dagger\hat{d}$ of a spinless level, according to the Hamiltonian $\hat{H}_{int} = \lambda(\hat{b}^\dagger + \hat{b})\hat{n}$. Such a model is recovered by replacing the operator $\hat{\sigma}_x$ with $\hat{\sigma}_z$, i.e. when spin-vibration interaction is parallel to the axis magnetization of the two leads so that the transport occurs through two separated spin-channels. On the other hand, the Hamiltonian of the dot has the form $\hat{H}_d = \varepsilon_0\hat{n} + \Delta\varepsilon_z\hat{\sigma}_z$ which represents, in the limit of vanishing coupling with the leads and with a single electron in the dot, the Rabi model, i.e. the simplest quantum model of interaction between an oscillator and spin.[72] Despite its simplicity, the Rabi-model is not integrable.

The Hamiltonian Eq. (6) is also similar to the one discussed in Refs. 73 and 74 although these previous works assumed the case of non-ferromagnetic leads and their analysis was focused on the transport in the low bias-voltage regime ($\sim I = GV$).

B. Phonon Green's function and occupation

1. *Phonon Green's functions*

Electrons tunneling through the CNTQD change the state of the nanomechanical resonator. The effect of nonequilibrium phonon state is taken into account by dressing the phonon Green's function with the polarization $\check{\Pi}(\varepsilon)$ to lowest order in λ. Additionally, we include a self energy $\check{\Sigma}_0(\varepsilon)$ modeling the coupling to an external bath. The Dyson equation in Keldysh space can then be written as

$$\check{D}(\varepsilon) = \check{d}(\varepsilon) + \check{d}(\varepsilon)\left(\check{\Pi}(\varepsilon) + \check{\Sigma}_0(\varepsilon)\right)\check{D}(\varepsilon)\,, \qquad (7)$$

in which the retarded and Keldysh Green's functions are defined as $D^R(t) = -i\theta(t)\langle[\hat{u}(t),\hat{u}(0)]\rangle$ and $D^K(t) = -i\theta(t)\langle\{\hat{u}(0),\hat{u}(t)\}\rangle$ with the deflection $\hat{u}$ and the commutator (anti-commutator) $[\,,\,]$ ($\{\,,\,\}$). We used the triangular Larkin-Ovchinnikov representation and we set $\hbar = k_B = 1$. The bare phonon propagators in Eq. (7) are given by

$$d^{R,A}(\varepsilon) = 2\omega/\left((\varepsilon \pm i\eta)^2 + \omega^2\right), \qquad (8)$$

$$d^K(\varepsilon) = -2\pi i(\delta(\varepsilon-\omega)+\delta(\varepsilon+\omega))\coth(\omega/(2T))) \qquad (9)$$

with an infinitesimal small real part η. To the first leading order λ in the spin-vibration interaction, the three components of the phonon self-energies for the spin-vibration interaction are given by:

$$\Pi^R(\varepsilon) = -i\frac{\lambda^2}{2}\sum_\sigma \big[G^K_{-\sigma}(\varepsilon')\circ G^A_\sigma(\varepsilon'-\varepsilon) + G^R_{-\sigma}(\varepsilon')\circ G^K_\sigma(\varepsilon'-\varepsilon)\big]\,, \qquad (10)$$

$$\Pi^K(\varepsilon) = -i\frac{\lambda^2}{2}\sum_\sigma \big[G^K_{-\sigma}(\varepsilon')\circ G^K_\sigma(\varepsilon'-\varepsilon) + G^R_{-\sigma}(\varepsilon')\circ G^A_\sigma(\varepsilon'-\varepsilon) + G^A_{-\sigma}(\varepsilon')\circ G^R_\sigma(\varepsilon'-\varepsilon)\big]\,. \qquad (11)$$

The symbol $\circ$ denotes the convolution product $a(x)\circ b(x-y) = \int_{-\infty}^{\infty}\frac{dx}{2\pi}a(x)b(x-y)$. Note that the interaction vertex due to the spin-vibration couples only spins of opposite sign. The electron Green's functions of the dot appearing Eqs. (10) and (11) are those associated with the unperturbed Hamiltonian and correspond to the exactly solvable problem of two dot levels coupled to the leads. These Green's functions are given by

$$G^{R,A}_\sigma = (g^{R,A^{-1}}_{0,\sigma} \pm i\Gamma^\sigma_l \pm i\Gamma^\sigma_r)^{-1}\,, \qquad (12)$$

$$G^K_\sigma = -2iG^R_\sigma(\Gamma^\sigma_l(1-2f_l)+\Gamma^\sigma_r(1-2f_r))G^A_\sigma\,, \qquad (13)$$

with the Fermi function of the left and right lead denoted by f_α.

To calculate the self energies $\check{\Sigma}_0$, we model the environment by the Caldeira Leggett model (see Appendix A). The coupling of the single oscillator to a bath of oscillators leads to the retarded and Keldysh self energies

$$\Sigma^R_0(\varepsilon) = -i\varepsilon/Q \qquad (14)$$

$$\Sigma^K_0(\varepsilon) = -2i\varepsilon\coth(\varepsilon)/Q\,, \qquad (15)$$

with the Quality-factor Q of the resonator.

Finally, we obtain the full Phonon Green's function by Eq. (7). As the interaction is small, we can expanded the retarded phonon propagators around $\varepsilon \lesssim \omega$. We define the damping as $\gamma_{tot}(\omega) = -\mathrm{Im}[\Pi^R(\omega)+\Sigma^R_0(\omega)]$, whereas the frequency renormalisation is $\Delta\omega = \mathrm{Re}[\Pi^R(\omega)+\Sigma^R_0]$ and $\tilde{\omega} = \omega + \Delta\omega$. The results are

$$D^R(\varepsilon) = \frac{2\omega}{\varepsilon^2 - \omega^2 - 2\omega(\Pi^R(\varepsilon)+\Sigma^R_0(\varepsilon))} \simeq \frac{1}{\varepsilon - \tilde{\omega} + i\gamma_{tot}} - \frac{1}{\varepsilon + \tilde{\omega} + i\gamma_{tot}}\,, \qquad (16)$$

$$D^K(\varepsilon) = D^R(\varepsilon)\Pi^K(\varepsilon)D^A(\varepsilon) \simeq \frac{\pi}{\gamma_{tot}}\left(\Pi^K(\varepsilon)+\Sigma^K_0(\varepsilon)\right)\left[\delta(\varepsilon-\tilde{\omega})+\delta(\varepsilon+\tilde{\omega})\right]. \qquad (17)$$

In the following we set $\tilde{\omega} \to \omega$.

2. Phonon occupation

The spin-polarized current drives the oscillator towards a nonequilibrium steady state $n = (i/8\pi)\int d\varepsilon D^K(\varepsilon) - 1/2$ which can be reduced to

$$\bar{n} = \frac{\gamma_0 n_B(\omega) + \gamma n}{\gamma_0 + \gamma}. \tag{18}$$

The steady state is reached by two competing processes. The first term corresponds to the interaction of the mechanical oscillator with the thermal bath with the damping $\gamma_0 = -\mathrm{Im}\,\Sigma_0^R(\omega) = \omega/Q$ and the Bose distribution $n_B(\omega)$. The second term is associated to the spin-vibration interaction leading to a damping γ and an occupation n given by ($s = \pm 1$)

$$\gamma = \sum_{\alpha\beta s} s\gamma^s_{\alpha\beta}\,, \tag{19}$$

$$n = \frac{1}{\gamma}\sum_{\alpha\beta s} s\gamma^s_{\alpha\beta} n_B(\omega + s(\mu_\alpha - \mu_\beta))\,. \tag{20}$$

Here we introduced the lead chemical potentials μ_α and

$$\gamma^s_{\alpha\beta} = \frac{\lambda^2}{2}\int \frac{d\varepsilon}{2\pi} T^s_{\alpha\beta}(\varepsilon,\omega) f_\alpha(\varepsilon)\left[1 - f_\beta(\varepsilon + s\omega)\right]\,, \tag{21}$$

with the Fermi function $f_\alpha(\varepsilon) = \{1 + \exp\left[(\varepsilon - \mu_\alpha)/T\right]\}^{-1}$, $L^\sigma_\alpha(\varepsilon) = 2\Gamma^\sigma_\alpha / \left[(\Gamma^\sigma_l + \Gamma^\sigma_r)^2 + (\varepsilon - \varepsilon_\sigma)^2\right]$ and

$$T^s_{\alpha\beta}(\varepsilon,\omega) = \sum_\sigma L^\sigma_\alpha(\varepsilon) L^{-\sigma}_\beta(\varepsilon + s\omega). \tag{22}$$

$\gamma^s_{\alpha\beta}$ corresponds to the rates for inelastic processes in which a spin flip occurs for one electron tunneling from lead α to lead β accompanied by the absorption ($s = +$) or emission ($s = -$) of an energy quantum of the vibron. Equation (19) also shows that the processes of absorption (emission) of a phonon give a positive (negative) contribution to γ. Therefore, for certain configurations, the resonator can be driven to a mechanical instability for which $\gamma_{tot} < 0$. As last point, we observe that our approximation on the self energy to the first order is valid if the coupling is sufficiently small, i.e. the mechanical damping $\gamma \ll \omega$. We focus on this regime in this work.

C. Electronic Green's function and current

The transport properties through the nanomechanical spin-valve with spin-vibration interaction are calculated by the Keldyh-Green's function technique. The coupling to the leads are taken into account to infinite order in the coupling $t_{\alpha\sigma}$. In order to understand the effect of the spin-vibration interaction, we calculate the correction to the current to first leading order in the coupling.[75,76]

The current operator through the left contact can be expressed as[75,76]

$$I_l = e\langle\frac{d\hat{N}_l}{dt}\rangle = \frac{2e}{h}\,\mathrm{Re}\left[t_{l\sigma}\sum_{k\sigma}\int_{-\infty}^{+\infty} d\varepsilon\, \mathcal{G}^<_{d\sigma,lk\sigma}(\varepsilon)\right]\,, \tag{23}$$

in which $\langle\ldots\rangle$ denotes the quantum statistical average[77,78] and $\mathcal{G}^<_{dlk}(\varepsilon)$ the Fourier transform of the Green's function $\mathcal{G}_{dlk}(t,t') = i\langle\hat{c}_{lk}(t')\hat{d}^\dagger(t)\rangle$. The corresponding Green's function in Keldysh space are defined as $\mathcal{G}_{dlk}(\tau,\tau') = -i\langle T_c\hat{c}_{lk}(\tau)\hat{d}^\dagger(\tau')\rangle$ with the time-ordering operator T_c on the Keldysh contour. Transforming from the contour variable τ to the real time and using the Larkin-Ovchinnikov rotation, we introduce the triagonal matrix representation $\check{\mathcal{G}}$ such that $\check{\mathcal{G}}$ is composed by only three components $\mathcal{G}^{R,A,K}$ (retarded, advanced, Keldysh). From diagrammatics, we obtain the Dyson equation $\check{\mathcal{G}}_{dl} = \check{\mathcal{G}}_{dd}\check{t}^*_l\check{g}_l$ where $\check{g}_{lk\sigma}$ denotes the Keldysh Green's function for vanishing tunneling in the Hamiltonian H_0. Inserting the Lesser element $\mathcal{G}^<_{dl} = (\mathcal{G}^K_{dl} - \mathcal{G}^R_{dl} - \mathcal{G}^A_{dl})/2$ of $\check{\mathcal{G}}_{dl}$ in the current (23) one obtains

$$I_l = \frac{e}{h}\sum_\sigma \Gamma^\sigma_l\,\mathrm{Re}\int d\varepsilon[i\mathcal{G}^K_{d\sigma,d\sigma}(\varepsilon) - 2i\,(1 - 2f_l(\varepsilon))\,\mathcal{G}^R_{d\sigma,d\sigma}(\varepsilon)]. \tag{24}$$

The problem then reduces to the calculation of the Green's function (neglecting the index dd) $\mathcal{G}^{K,R,A}_{\sigma\sigma}$. We expand the Green's function on the Keldysh contour $\mathcal{G}(\tau,\tau') = -i\langle T_c\hat{d}(\tau)\hat{d}^\dagger(\tau')\rangle$ to the order λ^2 treating the spin-vibration interaction as the perturbation. The result of the expansion can be written as $\mathcal{G}_{\sigma\sigma}(\tau,\tau') = G_\sigma(\tau,\tau') + G^{(2)}_{\sigma\sigma}(\tau,\tau')$, with the Green's function $G_\sigma(\tau,\tau')$ corresponding to the exact solution of the tunneling resonant problem for vanishing spin-vibration interaction [Eq. (12)]. Finally, we transform the contour variable to the real time and use the Larkin-Ovchinnikov transformation to represent the perturbation expansion in Keldysh space as

$$\check{\mathcal{G}}_{\sigma\sigma}(\varepsilon) = \check{G}_\sigma(\varepsilon) + \check{G}_\sigma(\varepsilon)\check{\Sigma}_{-\sigma-\sigma}(\varepsilon)\check{G}_\sigma(\varepsilon) \tag{25}$$

The elements of the self energies $\check{\Sigma}_{\sigma\sigma}$ due to the spin-vibration interaction in Eq. (25) are denoted as $\Sigma^{R,A,K}_{\sigma\sigma}$ and are given by

$$\Sigma^{R,A}_{\sigma\sigma}(\varepsilon) = D^{R,A}(\varepsilon')\circ G^K_\sigma(\varepsilon - \varepsilon') + D^K(\varepsilon')\circ G^{R,A}_\sigma(\varepsilon - \varepsilon'), \tag{26}$$

$$\Sigma^K_{\sigma\sigma}(\varepsilon) = \sum_{\zeta = R,A,K} D^\zeta(\varepsilon')\circ G^\zeta_\sigma(\varepsilon - \varepsilon') \tag{27}$$

with the Phonon Green's functions $D^{R,A,K}$ of Eqs. (16) and (17). The corrections to the current is finally obtained by inserting the retarded and Keldysh element of the perturbative expansion (25) into Eq. (24).

If we compare our results with the Anderson-Holstein model, we observe that for the Rabi-model here discussed, the tadpole diagrams to lowest order vanishes due the spin-flipping at the interaction vertex, see Fig. 3. Hence the expression in Eqs. (26) and (27) for the rainbow diagram in each spin-channel represents the unique contribution to the self-energy. On the other hand, the self-energy itself $\check{\Sigma}_{\sigma\sigma}$ is similar to the analytic expression for the Anderson-Holstein model,[62,67,75] albeit the spin-index due to the spin-flip scattering.

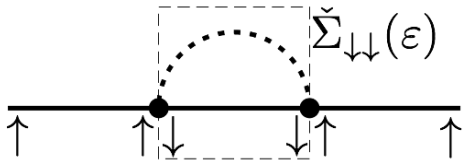

Figure 3. Rainbow diagram with spin-flip scattering. The diagram shows the term $\check{G}_\sigma\check{\Sigma}_{-\sigma-\sigma}\check{G}_\sigma$.

III. DAMPING OF THE OSCILLATOR AND PHONON OCCUPATION

An applied voltage drives the resonator in a nonequilibrium state. Additionally, we observe a mechanical instability setting in when the total damping rate is negative $\gamma_{tot} \leq 0$. In a previous work [52], we studied ground-state cooling for two polarized ferromagnets in the antiparallel configuration and discussed the dependence of the phonon occupation on the polarization and the energy separation ε_z.

Concerning the case of the parallel configuration we found that with same polarization $p_r = p$, $p_l = p$, the only effect of an applied voltage is to increase the phonon occupation. Cooling processes are overwhelmed by the heating ones as the spin-vibration interaction connects spin-up (down) electrons on the left lead with spin-down (up) electrons on the right leads resulting in a strong suppression of the rates associated to the cooling processes since the transmissions of Eq. (22) are proportional to $\Gamma_\alpha^+\Gamma_\beta^-$. However, if we relax the condition of same polarization, the phonon occupation can be cooled with low efficiency. The system also can become mechanical unstable. In the following, we focus on two additional issues: the mechanical instability for the antiparallel configuration and the cooling or heating for a single polarized lead.

In the Sec. III A we summarize our previous results. In Sec. III B we discuss the state of the mechanical resonator in the antiparallel configuration with same polarization. Since the inversion of the left and right polarizations with sgn(p)=-sgn(ε_z) is equivalent to a reversed voltage, we keep the polarization fixed to sgn(p)=sgn(ε_z) and $p_r = p$, $p_l = -p$ in the following discussion. This configuration allows for efficient cooling to the ground state and a strong heating of the resonator resulting in a mechanical instability corresponding to the operating regime in which phonon lasing has been discussed recently.[46] In Sec. III C we discuss cooling with a single polarized lead.

In a first step we consider a relatively large energy separation ε_z such that mainly either the spin-up or spin-down level is involved in transport associated with the processes shown in Fig. 4(a)-(d). In the second step, we study the phonon occupation close to resonance $\varepsilon_z = \omega$. This regime is sketched in Fig. 4 (e) and (f).

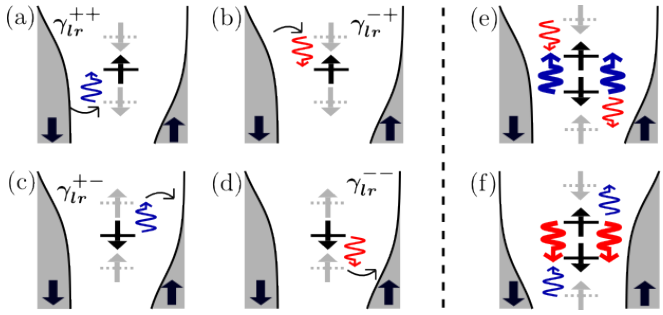

Figure 4. Schematic picture for the spin-flip processes with rate $\gamma_{lr}^{s\sigma}$ for fully polarized ferromagnets. In (a)-(d) a single level contributes to transport and leads to absorption (upwards blue arrows) or emission (downward red arrows) of a vibrational energy quantum. In (e) and (f) the resonant condition $\varepsilon_z = \omega$ is fulfilled. In (e), optimal ground state cooling of the oscillator is achieved. In (f) a strong heating occurs which is precursor of a mechanical instability of the oscillator.

A. Summary of previous results

Hereafter, to be define, we assume $\varepsilon_z > 0$ with $p_l < 0$, $p_r > 0$. In the high temperature regime $T \gg \Gamma_\alpha^\sigma$ and high Zeeman splitting $T \ll \varepsilon_z$, one can use an analytic approximation for the rates $\gamma_{\alpha\beta}^s$, which is in excellent agreement with the full results of Eq. (21). The Lorentzian functions appearing in Eq. (21) can be treated separately as δ-functions in the integral and we can cast each rate as the sum of two rates $\gamma_{\alpha\beta}^s \simeq \sum_\sigma \gamma_{\alpha\beta}^{s\sigma}$, for tunneling through the dot level σ, respectively. The additional index σ indicates that the tunneling processes involves the dot level $\sigma = \pm$. They read

$$\gamma_{\alpha\beta}^{s\sigma} = \frac{\lambda^2}{\Gamma_l^\sigma + \Gamma_r^\sigma}\Big\{\Gamma_\alpha^\sigma\Gamma_\beta^{-\sigma}T_+^{s\sigma}f_\alpha(\varepsilon_\sigma)\left[1 - f_\beta(\varepsilon_\sigma + s\omega)\right] + \Gamma_\alpha^{-\sigma}\Gamma_\beta^\sigma T_-^{s\sigma}f_\alpha(\varepsilon_\sigma - s\omega)\left[1 - f_\beta(\varepsilon_\sigma)\right]\Big\} \tag{28}$$

with $T_\pm^{s\sigma} = 1/\left[(\Gamma_l^{-\sigma} + \Gamma_r^{-\sigma})^2 + (\sigma\varepsilon_z \pm s\omega)^2\right]$. For fully polarized ferromagnetic leads one of the two terms of the processes in $\gamma_{\alpha\beta}^s$ vanish. Examples of the processes associated to the rate Eq. (28) are shown in Fig. 4(a)-(d) for each of the two spin levels.

In the high-voltage limit $eV \gg T$ ($e > 0$), we can neglect the processes $\gamma_{rl}^s \simeq 0$ being $V > 0$ as electrons tunneling from the right lead are Pauli blocked. The total damping then reduces to the sum of only two processes $\gamma \simeq \gamma_{lr}^+ - \gamma_{lr}^-$ and the expression of n simplifies to the average distribution resulting from these two competing processes

$$n \simeq \frac{\gamma_{lr}^+ n_B(\omega + eV) - \gamma_{lr}^- n_B(\omega - eV)}{\gamma_{lr}^+ - \gamma_{lr}^-} \simeq \frac{\gamma_{lr}^-}{\gamma_{lr}^+ - \gamma_{lr}^-}\,. \tag{29}$$

The second step in Eq. (29) holds for $eV \gg \omega$, when the nonequilibrium phonon occupation is completely ruled by

the ratio $\gamma_{lr}^{+}/\gamma_{lr}^{-}$. Although in the region of stability defined by $\gamma_{lr}^{+} > \gamma_{lr}^{-}$ the total damping is always positive, n can show heating or cooling: for $\gamma_{lr}^{+} \gtrsim \gamma_{lr}^{-}$ the mechanical oscillator is almost undamped and it is actively heated to $n \gtrsim n_B(\omega)$ whereas for $\gamma_{lr}^{+} \gg \gamma_{lr}^{-}$ the dominant emission processes yield an efficient cooling of the oscillator.

Strong cooling is achieved at resonance when $\varepsilon_z \simeq \omega$. From the full rates Eq. (21), we can estimate the lower limit for maximal cooling. For fully polarized ferromagnets with $p_l = -1$ and $p_l = 1$ and in the limit $eV \gg (T, \omega, \varepsilon_0)$, the Fermi function are $f_l \simeq 1$ and $f_r \simeq 0$ and the phonon occupation of Eq. (20) becomes $n \simeq (\Gamma/\omega)^2$. The processes corresponding to maximal cooling are shown in Fig. 4(e). By reversing the voltage, we pass to the regime of strong heating leading to a mechanical instability [Fig. 4(f)] which we discuss in the next section.

B. Instability

In Fig. 5(a) we consider the regime of a single level involved in transport and fully polarized ferromagnets. We set the left chemical potential $\mu_l = \varepsilon_0$ and $\mu_r = \varepsilon_0 - eV$ such that for $eV > 0$ ($eV < 0$), the spin-down (up) level mainly contributes to transport. For positive voltage $V > 0$, the oscillator can be cooled or heated as discussed in previous work Ref.[52]. For negative voltage we found that the oscillator is strongly heated as increasing the bias voltage. Eventually the system approaches a mechanical unstable region: the total damping becomes negative $\gamma_{tot} = \gamma + \gamma_0 < 0$.

The different behaviors for $eV > 0$ and $eV < 0$ can be understood by considering the rates of Eq. (28). Since $\Gamma_l^{+} = \Gamma_r^{-} = 0$ one of the two terms appearing in Eq. (28) vanish for each spin channel. For symmetric contacts $\Gamma_l^{-} = \Gamma_r^{+} = \Gamma$ and setting $T_{\pm}^{s} = \lambda^2\Gamma/[\Gamma^2 + (s\omega \pm \varepsilon_z)^2]$, the single spin-channel rates are given by

$$\gamma_{lr}^{s\sigma} = T_{-}^{s}\, f_l(\varepsilon_\sigma - s\omega\delta_{\sigma+})\,[1 - f_r(\varepsilon_\sigma + s\omega\delta_{\sigma-})]\ , \quad (30)$$

$$\gamma_{rl}^{s\sigma} = T_{+}^{s}\, f_r(\varepsilon_\sigma - s\omega\delta_{\sigma-})\,[1 - f_l(\varepsilon_\sigma + s\omega\delta_{\sigma+})]\ . \quad (31)$$

In the regime $eV > 0$ and the high-voltage limit, we can approximate the phonon occupation as $n = \gamma_{lr}^{--}/(\gamma_{lr}^{+-} - \gamma_{lr}^{--})$ since only the spin-down level is involved in transport. Cooling occurs for $\gamma_{lr}^{+-} \gg \gamma_{lr}^{--}$ while heating occurs when $\gamma_{lr}^{+-} \gtrsim \gamma_{lr}^{--}$. The crossover from cooling to heating depends on the Fermi function $(1 - f_r(\varepsilon_- + s\omega))$ and the factor T_{-}^{s} in Eq. (30). Note that, the total damping $\gamma_{tot} = \gamma_{lr}^{+-} - \gamma_{lr}^{--}$ is positive for $eV > 0$ since the difference in the Fermi function in γ_{lr}^{+-} and γ_{lr}^{--} is positive and additionally $T_{-}^{+} \gtrsim T_{-}^{-}$. Therefore, for $eV > 0$, the systems remains stable by increasing the voltage and the transition from cooling to heating can be understood in the following picture. At low temperature, the electrons tunnel from the left lead to the spin-down level accompanied by a spin-flip tunneling to the right lead. At $\mu_r \gtrsim \varepsilon_-$ the processes of cooling (absorption of a phonon) dominate over the processes of heating (emitting a phonon), since the heating processes are suppressed by the Fermi function. When $\mu_r \lesssim \varepsilon_-$, the heating processes are possible and the phonon occupation increases. At finite temperature, the thermal broadening of the Fermi functions causes a smooth transition between the regimes of cooling and heating.

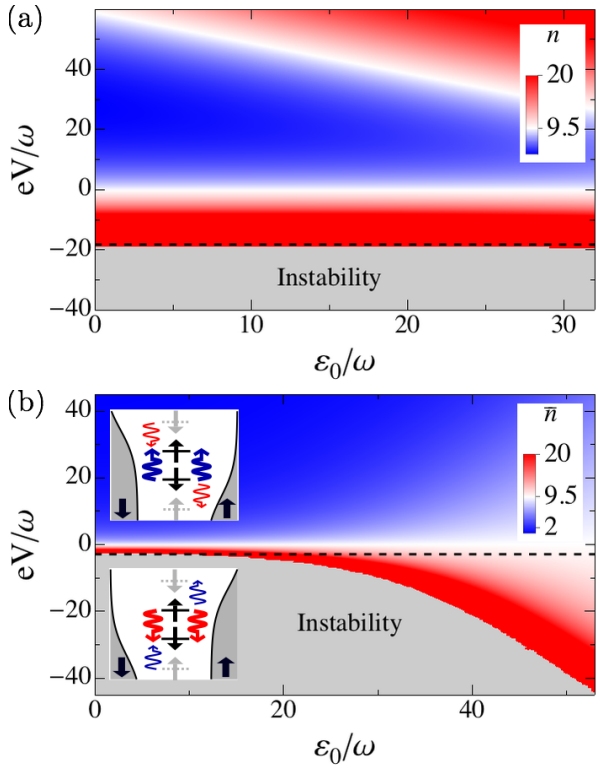

Figure 5. Phonon occupation as function of the bias voltage V and gate voltage ε_0. The parameters are $p_l = -1$ and $p_r = 1$, $\Gamma_l = \Gamma_r = 0.2\omega$, and $T = 10\omega$. White corresponds to $n_B(\omega)$. (a) Vanishing external damping $\gamma_0 = 0$, $\varepsilon_z = 10T$, $\mu_r = \varepsilon_0 - eV$, and $\mu_l = \varepsilon_0$. (b) Resonant regime $\varepsilon_z = \omega$ with $\gamma_0 = 10^{-5}\omega$, $\lambda/\omega = 0.01$, and $\mu_{l,r} = \varepsilon_0 \pm eV/2$.

We now turn the case $eV < 0$. In the high voltage approximation, the relevant processes are $\gamma_{rl}^{s\sigma}$ and the phonon occupation is given by $n = \gamma_{rl}^{-+}/(\gamma_{rl}^{++} - \gamma_{rl}^{-+})$. The electrons tunnel from the right lead to the dot and finally to the left accompanied by a spin-flip. In comparison with the case $eV > 0$, now the transmission for heating is larger than the transmission for cooling ($T_{+}^{-} \gtrsim T_{+}^{+}$) indicating that in this regime the total damping can also be negative resulting in an instability of the resonator. The instability in the single channel approximation is attributed to the different magnitude of the transmissions. In the high-temperature limit $f_r \simeq 1$ and $f_l = 0$ such that the total damping reduces to $\gamma_{tot} = T_{+}^{+} - T_{+}^{-} < 0$.

From Eq. (30) we can also discuss the onset of the instability. Since the instability occurs at relatively small voltages, we can not use the high-voltage approximation. In the limit of $\varepsilon_z \gg \omega$, the total damping reduces to

$\gamma_{tot} = \gamma_{rl}^{++} - \gamma_{rl}^{-+} + \gamma_{lr}^{++} - \gamma_{lr}^{-+}$. Then, setting $\gamma_{tot} = 0$, we obtain the equation for the onset of instability $eV = -T\ln[1+(1/T)(\omega+\varepsilon_z/2)]$ to leading order in T/ε_z. The line does not depend on ε_0 as shown in Fig. 5(a).

In the resonant case, the phonon occupation is shown in Fig. 5(b) with an intrinsic damping of $Q = 10^5$, a spin-vibration coupling of $\lambda = 0.01\omega$ and symmetrically applied voltage. Since now both levels are involved in transport we consider Eq. (21) to discuss the instability. In the high-voltage limit, the only transmissions of Eq. (22) giving a relevant contribution to the current are T_{lr}^s for $\mu_l > \mu_r$ and T_{rl}^s for $\mu_l < \mu_r$. In the first case, $T_{lr}^+ > T_{lr}^-$, such that the system is stable. In this region we obtain strong cooling as discussed in Ref. [52]. In the second case $\mu_l < \mu_r$, $T_{rl}^+ < T_{rl}^-$ and for sufficient large voltages, the total damping rate becomes negative. An intrinsic damping reduces the parameter range for which we obtain the instability. Anyway, as shown in Fig. 5(b), the system becomes unstable even for relatively small voltages.

The strong heating and instability obtained for the resonant regime can be explained as follows. The emission processes for each spin channel are now the same as the virtual levels $\varepsilon_- - \omega$ and $\varepsilon_- + \omega$, which are involved in the spin-flip tunneling for heating, coincide, respectively, to the real dot spin levels ε_+ and ε_-. This yields a strong enhancement of the (transmission) function T_-.

In the high-temperature limit $T \gg (eV, \varepsilon_0, \varepsilon_z)$, we can expand the Fermi functions in Eq. (21) to lowest order in ε/T and perform the integrations. As a result we obtain the line for which the total damping rate becomes negative

$$eV = -\frac{4\Gamma^2+\omega^2}{\omega^2} - 16\,T\,\Gamma\frac{4\Gamma^2+\omega^2}{Q\lambda^2\omega} \tag{32}$$

This line in plotted in Fig. 5 (b) and agrees with the onset of the instability for small ε_0/ω. For larger ε_0/ω, the approximation of $T \gg \varepsilon_0$ gradually breaks down and the approximation becomes less accurate. Finally, we found that the instability also occurs at finite polarization.

In the regime of instability, our model of a harmonic oscillator breaks down. Even before reaching this regime, the oscillator can store enough mechanical energy such that its dynamics is characterized by oscillations of large amplitude. In this regime, anharmonic effects play an important role and the harmonic approximation for the resonator breaks down. Additionally, in this regime the Q-factor can also depend on further parameter as the displacement of the resonator.

C. Single polarized lead

In this section we discuss the modification of the cooling when only a single lead is polarized. We restrict the discussion to a left polarized lead ($p_l \neq 0$) and a normal right lead ($p_r = 0$). This configuration is equivalent to setting the reversed left polarization on the right lead and the opposite voltage. The processes $\gamma_{lr}^{s\sigma}$ for $p_l = -1$ are sketched in Fig. 4 except that the polarization on the right lead must be set to zero. Since $p_r = 0$, we have to include additionally the processes $\gamma_{rr}^{\pm}$ and at $p_l > -1$, the processes $\gamma_{ll}^{\pm}$ which corresponds to an electron tunneling on the dot, flipping its spin and then coming back to its initial lead. In the high-voltage approximation, the phonon occupation of Eq. (20) can then be written as

$$n \simeq \frac{\gamma_{lr}^-(p_l) + n_B(\gamma_{ll}(p_l)+\gamma_{rr})}{\gamma_{lr}^+(p_l) - \gamma_{lr}^-(p_l) + \gamma_{ll}(p_l) + \gamma_{rr}}. \tag{33}$$

with $\gamma_{\alpha\alpha}=\gamma_{\alpha\alpha}^+-\gamma_{\alpha\alpha}^-$. For $\gamma_{lr}^+(p_l)-\gamma_{lr}^-(p_l) \gg \gamma_{ll}(p_l)+\gamma_{rr}$, we can write (33) as $n\simeq n(p=1)+(n_B-n(p=1))(\gamma_{ll}(p_l)+\gamma_{rr})/(\gamma_{lr}^+(p_l)-\gamma_{lr}^-(p_l))$ with the phonon occupation $n(p=1)$ for fully polarized left and right leads $p = p_l = -p_r$ given by Eq. (29). From the expansion one can see that the effect of a right normal lead or a finite polarization on the left lead is to drive the phonon occupation towards the equilibrium occupation.

The minimal phonon occupation $\bar{n}_{min}$ as a function of the left polarization p_l and the energy separation ε_z is shown in Fig. 6(a) and (b), respectively. For $p_l = -1$, the differences to the case of two fully polarized ferromagnets are the processes $\gamma_{rr}^{\pm}$ which try to drive the resonator at thermal equilibrium. However, the processes γ_{rr}^+ and γ_{rr}^- only contribute to the total damping close to the right chemical potential due to the factor $f_r(\varepsilon)(1-f_r(\varepsilon+s\omega))$ in Eq. (22). Therefore, if the energy separation is close to resonance and $\mu_l \gg \varepsilon_0 \pm \varepsilon_z \gg \mu_r$, these processes are strongly suppressed and cooling close to the ground state can still be achieved. When $p_l > -1$ additionally the processes $\gamma_{ll}^{\pm}$ drive the resonator to equilibrium and cooling is suppressed.

In Fig. 6(a), the minimal phonon occupation remains at equilibrium below a certain threshold polarization below which the resonator is heated. This behavior is contrary to the case of two fully polarized ferromagnets where the minimal occupation decreases continuously as reducing the polarization. This relies on the fact that the cooling processes must overcome the right-right spin-flip processes. These processes are characterized by the rate γ_{rr} which is independent of p_l as shown in Eq. (33).

In Fig. 6(b) we show the cooling for a single polarized lead. In the configuration discussed above the electrons flip the spin while tunneling from the left lead to the dot. After the spin-flip the electrons are absorbed in the right lead. Therefore, the left lead acts as a source for injection of spin-polarized electrons, see Fig. 4(a,b) without preventing the possibility of occurring cooling processes in the opposite lead. A similar argument holds when we consider $p_l = 0$ and $p_r = -1$. In this case, spin-up and spin-down electron can enter the contact and the right lead acts as filter selecting only spin-down electrons.

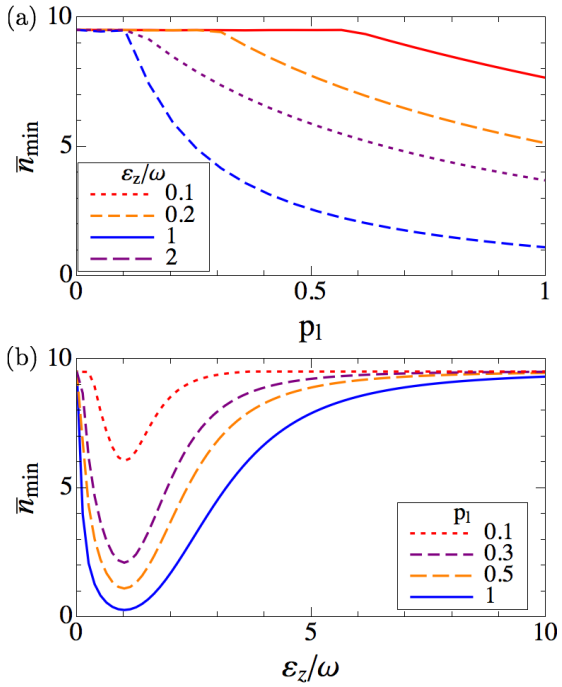

Figure 6. Minimal phonon occupation for one polarized lead as a function of p_l (a) and ε_z (b). Parameters: $\Gamma_l = \Gamma_r = 0.2\Gamma$, $T = 10\omega$, $Q = 10^4$ and $\lambda = 0.05\omega$.

IV. CURRENT

In this section, we study the transport properties of the carbon nanomechanical resonator in contact with ferromagnetic leads. We focus on weak spin-vibration interaction and perform a perturbation expansion to leading order in λ using a similar approach as in Refs. 67, 73 and 79.

We calculate the signature in the current of the spin-vibration interaction for two cases. In section IV A, we assume that the resonator is strongly coupled to the external bath such that $\gamma_0 \gg \gamma$. In other words, the time for thermal relaxation is much smaller than the time associated to the inelastic spin flip processes to set the oscillator in an unequilibrated state. The resonator occupation can be described by the Bose distribution function. This regime is referred to as the regime of strong damping (thermal equilibrated vibration). In section IV B, we consider a carbon nanotube with a high quality factor of $Q = 10^5$. In this regime the resonator is driven by the current itself towards the nonequilibrium phonon occupation (unequilibrated vibration).

A. Current with equilibrated vibration

The general result for the current can be written in terms of an elastic current I_0, an elastic correction I_{ec} and an inelastic current I_{in},[67,79]

$$I = I_0 + I_{ec} + I_{in}. \tag{34}$$

The elastic part describes the current not interacting with the oscillator and is given by

$$I_0 = \frac{e}{h}\int d\varepsilon \sum_\sigma \Gamma_l^\sigma \Gamma_r^\sigma |G_\sigma(\varepsilon)|^2 \left(f_l(\varepsilon) - f_r(\varepsilon)\right). \tag{35}$$

We first consider the elastic correction to the conductance and in a second step discuss the differential conductance for equilibrated vibrations.

1. *Elastic correction with thermalized vibration*

The elastic correction of our model Hamiltonian can written as ($\varepsilon_s = \varepsilon + s\omega$)

$$I_{ec} = \lambda^2 \frac{2e}{h}\int d\varepsilon \left(\sum_s s[n_B(s\omega) T_{ec}^s(\varepsilon) + \sum_\alpha T_{ec}^{\alpha,s}(\varepsilon) f_\alpha(\varepsilon_s)] - \int \frac{d\varepsilon'}{2\pi} {\rm Re} D^R(\varepsilon') \sum_\alpha T_{ec}^\alpha(\varepsilon,\varepsilon') f_\alpha(\varepsilon - \varepsilon') \right) \left(f_l(\varepsilon) - f_r(\varepsilon)\right), \tag{36}$$

with the transmission defined as

$$T_{ec}^s(\varepsilon) = 4\sum_\sigma |G_\sigma^R(\varepsilon)|^2 \Gamma_l^\sigma \Gamma_r^\sigma {\rm Re}[G_\sigma^R(\varepsilon) G_{-\sigma}^R(\varepsilon_s)], \tag{37}$$

$$T_{ec}^{\alpha,s}(\varepsilon) = 4\sum_\sigma \Gamma_l^\sigma \Gamma_r^\sigma \Gamma_\alpha^{-\sigma} |G_\sigma^R(\varepsilon) G_{-\sigma}^R(\varepsilon_s)|^2 {\rm Im}[G_\sigma^R(\varepsilon)], \tag{38}$$

$$T_{ec}^\alpha(\varepsilon) = 8\sum_\sigma \Gamma_l^\sigma \Gamma_r^\sigma \Gamma_\alpha^{-\sigma} |G_\sigma^R(\varepsilon) G_{-\sigma}^R(\varepsilon - \varepsilon')|^2 {\rm Re}[G_\sigma^R(\varepsilon)]. \tag{39}$$

In the above formula, the integral of the retarded Green's function has to be understood as the principle value.

At $T = 0$, the elastic correction $G = dI_{ec}/dV|_{V=0}$ reduces to

$$\frac{G_{ec}}{G_0} = \sum_{s\sigma} \frac{2\lambda^2 \Gamma^{-\sigma} \Gamma_l^\sigma \Gamma_r^\sigma \varepsilon_\sigma}{\left(\Gamma^{\sigma 2} + \varepsilon_\sigma^2\right)^2 \left(\Gamma^{-\sigma 2} + (\varepsilon_{-\sigma} + s\omega)^2\right)} \left(\frac{\varepsilon_{-\sigma} + s\omega}{\Gamma^{-\sigma}} \left(1 + \frac{2s}{\pi} \tan^{-1}\left(\frac{\varepsilon_{-\sigma}}{\Gamma^{-\sigma}}\right)\right) - \frac{s}{\pi} \ln\left(\frac{\omega^2}{\varepsilon_{-\sigma}^2 + \Gamma^{-\sigma 2}}\right)\right). \tag{40}$$

In a process contributing to the elastic correction to the conductance, an electron tunnels through the junction by virtually exciting the resonator. The resonator is excited by an emission (absorption) of a vibron followed by an absorption (emission) of a vibron and ends up at the same energy as the initial state. The obtained behavior is contrary to the one obtained in the Holstein

model of spinless electrons in which these processes always have the effect of increasing the conductance at zero temperature.

In Fig. 7, we show the elastic conductance Eq. (40) at zero temperature for the parallel and antiparallel configuration at $\omega = 5\Gamma$. The asymmetry of the elastic correction as a function of ε_0/Γ stems from the polarization of the ferromagnetic leads. In the parallel configuration the transport through the spin-up level is enhanced compared to the transport through the spin-down level since the majority charge carriers are spin-up electrons, thus leading to a larger conductance at the spin-up level. However, for the anti- parallel configuration, there are always electrons of the majority and minority spin involved giving raise to a symmetric and a suppression of the conductance. We notice that the correction is negative in the range $|\varepsilon_0| < \varepsilon_z/2$. This can be understood in the following way. Without the spin-vibration interaction, the spin-up and spin-down channel do not mix. When the spin-vibration is considered, an electron of spin up can tunnel from one lead to another one either through the dot level with spin-up or through the dot level with spin down due to the elastic spin-flip, see Fig. 3. This leads to a Fano interference effect with negative correction to the conductance in the range $|\varepsilon_0| < \varepsilon_z/2$.

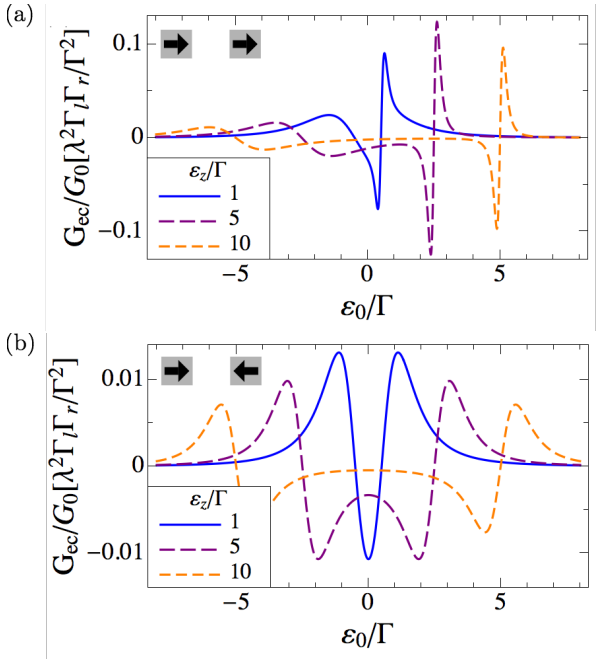

Figure 7. Conductance from elastic correction for parallel (a) and antiparallel (b) configuration for $T = 0$ and symmetric coupling to the leads. The parameters $\varepsilon_z = 5\Gamma$, $p_l = p_r = 0.8$.

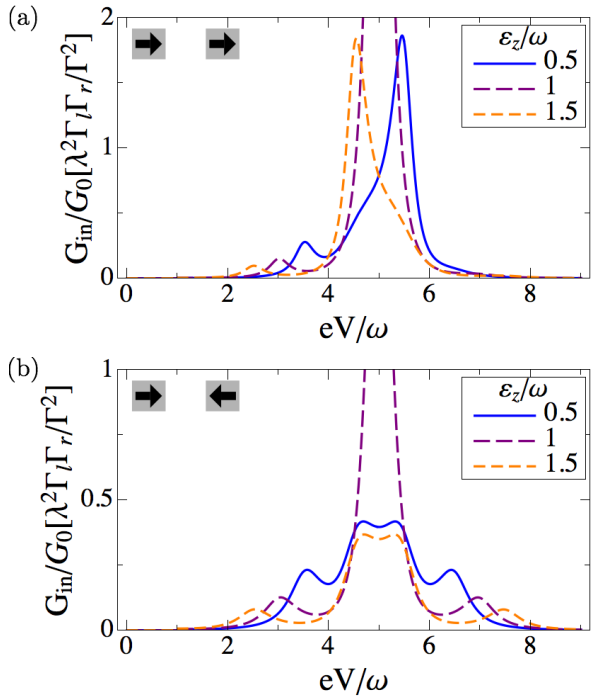

Figure 8. Inelastic contribution to differential conductance at zero temperature and $\varepsilon_0 = 2\omega$, $p_l = p_r = 0.4$, $\Gamma_l = \Gamma_r = 0.2\omega$ and the voltage is applied symmetrically. (a) Parallel configuration (b) Antiparallel configuration

2. *Inelastic current with equilibrated vibration*

In inelastic current can be written in terms of the rates $\gamma^s_{\alpha\beta}$ of Eq. (21) as

$$I_{in} = \frac{2e}{\hbar}\sum_s s n_B(s\omega)\left(\gamma^s_{lr} - \gamma^s_{rl}\right). \tag{41}$$

If the voltage is increased transport is possible via emission and absorption of phonons. At zero temperature the threshold voltage for an emission of a vibron is $eV = \omega$. As we calculated the inelastic current to lowest order in the coupling, only single phonon processes are taken into account. The differential conductance $G = dI_{in}/dV$ at zero temperature can be written as

$$\frac{G_{in}}{G_0} = \frac{\lambda^2}{4}\sum_{\sigma\alpha} L^{\sigma}_{\alpha}(\mu_\alpha) L^{-\sigma}_{-\alpha}(\mu_\alpha - \alpha\omega)\theta(\mu_l - \mu_r - \omega). \tag{42}$$

Fig. 8 (a) and (b) show the inelastic differential conductance at zero temperature in the parallel and antiparallel configuration respectively. The voltage is applied symmetrically $\mu_l = eV/2$ and $\mu_r = -eV/2$, the energy level on the dot is set to $\varepsilon_0 = 2\omega$ and the polarization is $p = p_r = p_l = 0.4$ for the parallel configuration and $p = p_r = -p_l = 0.4$ for the antiparallel configuration. In Fig. 8 the inelastic processes can occur at the voltages $eV/2 = \varepsilon_\pm$ and $eV/2 = \varepsilon_\pm + \omega$. The first peak

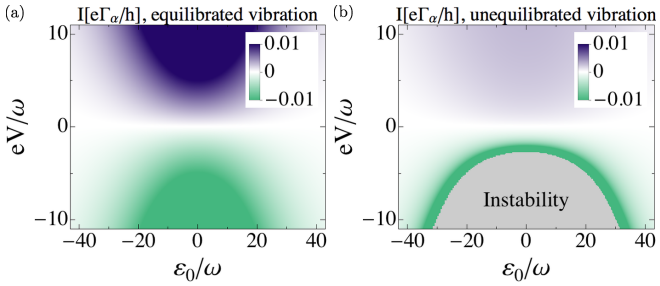

Figure 9. (Colors online) Inelastic current for equilibrated (a) and unequilibrated vibration (b) for fully polarized ferromagnets at resonance $\varepsilon_z = \omega$, $T = 10\omega$, $\Gamma = 0.2\omega$, $\lambda = 0.01\omega$ and $Q = 10^5$.

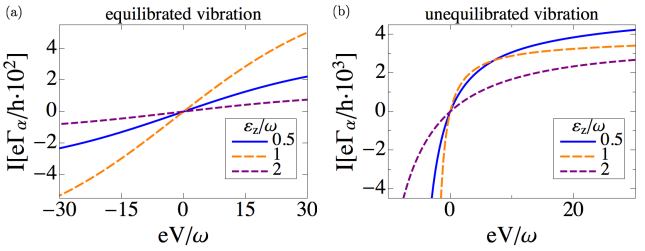

Figure 10. Current for equilibrated (a) and unequilibrated vibration (b) for fully polarized ferromagnets, $T = 10\omega$, $\varepsilon_0 = 0$, $\Gamma = 0.2\omega$, $\lambda = 0.01\omega$ and $Q = 10^5$.

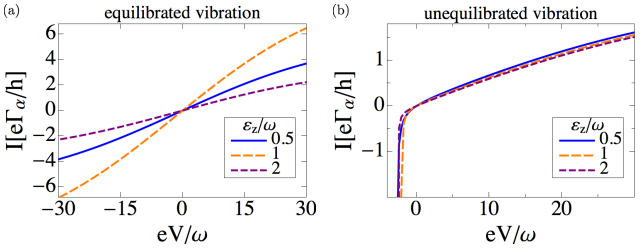

Figure 11. Current for equilibrated (a) and unequilibrated vibration (b) for $p = 0.5$, $T = 10\omega$, $\varepsilon_0 = 0$, $\Gamma = 0.2\omega$, $\lambda = 0.2\omega$ and $Q = 10^5$.

appears due to the resonance of the left Fermi level with the spin-down level on the quantum dot ($eV/2 = \varepsilon_-$). In this process a spin-down electron is transferred to the quantum dot followed by a spin-flip and an emission of a vibron at the right barrier. When the voltage is increased, a second peak arises due to inelastic spin-flip scattering at the left barrier. This peak is attributed to a resonance condition $eV/2 = \varepsilon_- - \omega$. In this case a spin-up electron flips the spin and is transferred to the right lead. These two processes are repeated if the voltage is further increased and the Fermi energy in the left lead is in resonance with the spin-up level of the quantum dot. At resonance $\varepsilon_z = \omega$, the differential conductance is strongly increased compared to the case out of resonance. Note that the strong coolmakiing in Fig. 5(b) is related to the large peak at resonance in Fig. 8(b).

B. Current with unequilibrated vibration

In this section, we discuss the current for the case of unequilibrated vibration. The current is given by the same Eqs.(34), (35), (36) and (41) in which the thermal Bose distribution inside the integral is replaced by $\bar{n}$. For oscillators with very high quality factor, we have that $\bar{n}$ is essentially n.[80] We find clear signatures of the nonequilibrium phonon occupation and in particular a strong suppression of the current when the resonator is strongly cooled.

In Fig. 9(a) and (b), we show the current at resonance for equilibrated and unequilibrated vibration respectively. We consider fully polarized ferromagnets, $T = 10\omega$ and $\Gamma = 0.2\omega$. The nonequilibrium phonon occupation corresponding to the current in 9(b) with $\lambda = 0.01\omega$ and $Q = 10^5$ is shown in Fig. 5(b) for $\varepsilon_0/\omega > 0$. Note that in the case of fully polarized ferromagnets, the current is complete carried by the inelastic processes of Eq. (34). By comparison of Fig. 9(a) and (b), we observe that the current for unequilibrated vibration is strongly asymmetric as a function of eV/ω. Furthermore, for $eV > 0$, the current in 9(b) is strongly suppressed compared to the case of equilibrated vibration. The decrease of the current occurs due to the cooling of the oscillator close to the ground state in this regime and the associated suppression of processes exciting electrons. For $eV < 0$, the current is strongly increased and the system becomes unstable. The current mainly follows the nonequilibrium phonon occupation of Eq. 9(b) and therefore serves as an indication of the nonequilibrium occupation and the spin-vibration interaction.

In Fig. 10 we compare the current for equilibrated vibration with the current for unequilibrated vibration including a damping of $Q = 10^5$ and a coupling $\lambda = 0.01\omega$. We consider fully polarized ferromagnets and different energy separations ε_z. The parameters are choose the same as in Fig. 5(b) and we plot the current along the line $\varepsilon_0 = 0$. In the case of equilibrated vibration, the current at resonance is larger than the current out of resonance. For unequilibrated vibration, the current is stronger suppressed at resonance, and hence also strongly reduces the current.

In Fig. 11 (a) and (b), we compare the current for equilibrated and unequilibrated vibration at $p_l = p_r = 0.5$. Additionally to the inelastic current, now also the elastic current and the elastic correction contribute to transport. In Fig. 11, we set $\lambda = 0.2\omega$ for large spin-orbit coupling as recently reported in Ref. 81 and observe the asymmetry of the current as well the instability where the current sharply decreases.

V. SUMMARY

In summary, we studied the steady-state phonon occupation in a suspended carbon nanotube quantum dot in contact with ferromagnetic leads. We have shown that the spin-vibration interaction induced by the spin-orbit coupling or a magnetic gradient can be exploited to cool and heat the flexural mode or drive the resonator to to an instability. Strong cooling can even be achieved for moderate polarizations, weak spin-vibration interaction and a single polarized lead. The current shows characteristic features of the nonequilibrium phonon occupation and directly can be exploited to demonstrate the presence of the spin-vibration interaction and the non-therrmal phonon occupation of the resonator.

ACKNOWLEDGMENTS

This research was kindly supported by the EU FP7 Marie Curie Zukunftskolleg Incoming Fellowship Programme, University of Konstanz (Grant No. 291784) the DFG through SFB 767 and BE 3803/5.

Appendix A: Phonon self-energy for the vibration-environment coupling

We consider a mechanical oscillator coupled to the environment which is described as an ensemble of harmonic oscillator (the Caldeira-Leggett model)

$$\hat{H} = \hbar\omega\hat{b}^\dagger\hat{b} + (\hat{b}^\dagger + \hat{b})\sum_n \lambda_n(\hat{b}_n^\dagger + \hat{b}_n) + \sum_n \hbar\omega_n\hat{b}_n^\dagger\hat{b}_n\,. \quad \text{(A1)}$$

As the Hamiltonian is quadratic, the model is exactly solvable: The phonon self-energy is composed by only one irreducible diagram. For instance, in the frequency space, the retarded self energy is given by

$$\Pi_{en}^R(\varepsilon) = \sum_n \lambda_n^2\left(\frac{1}{\varepsilon - \hbar\omega_n + i\eta} - \frac{1}{\varepsilon + \hbar\omega_n + i\eta}\right). \quad \text{(A2)}$$

To mimic the dissipation, the ensembles of oscillators form a bath with a continuos spectrum. Then, by replacing the sum with an integral over the frequencies and approximating $\Pi_{en}^R(\varepsilon) \simeq \Pi_{en}^R(\omega)$, we obtain

$$\gamma_0 = -\text{Im}\;\Pi_{en}^R(\omega) = \omega/Q\,, \quad \text{(A3)}$$

$$\Pi_{en}^K(\omega) = 2i\text{Im}\;\Pi_{en}^R(\omega)\text{coth}(\omega)\,, \quad \text{(A4)}$$

with Q the quality factor of the oscillator.

Appendix B: Appendix

The retarded self energy in Eq. (26) can be calculated analytically at zero temperature. For completeness and comparison, we give here the expression for the real and imaginary part. These expressions agree with the results of Ref. [67] when our model reduces to the Holstein model albeit with the generalized spin index.

$$\text{Re}\;\Sigma_{\sigma\sigma'}^R(\varepsilon) = \sum_{\alpha,s}\frac{\delta_{\sigma\sigma'}\lambda^2\Gamma_\alpha^\sigma}{(\varepsilon - \varepsilon_{-\sigma} - s\omega)^2 + \Gamma^{\sigma\sigma 2}}\left(\frac{\varepsilon - \varepsilon_\sigma - s\omega}{\Gamma^{\sigma\sigma}}\right.$$
$$\left.\left(\frac{1}{2} + \frac{s}{\pi}\tan^{-1}\frac{\varepsilon_\sigma - \mu_\alpha}{\Gamma^{\sigma\sigma}}\right) + \frac{s}{\pi}\ln\frac{|\varepsilon - s\omega - \mu_\alpha|}{\sqrt{(\varepsilon_\sigma - \mu_\alpha)^2 + \Gamma^{\sigma\sigma 2}}}\right), \quad \text{(B1)}$$

and

$$\text{Im}\;\Sigma_{\sigma\sigma'}^R = \sum_{\alpha,s}\frac{-\lambda^2\delta_{\sigma\sigma'}\Gamma_\alpha^\sigma\theta(s(\epsilon - \mu_\alpha) - \omega)}{(\varepsilon - s\omega - \varepsilon_\sigma)^2 + \Gamma^{\sigma\sigma 2}}. \quad \text{(B2)}$$

Here, we use the notation $\Gamma^{\sigma\sigma'} = \Gamma_l^\sigma + \Gamma_r^{\sigma'}$.

[1] M. Roukes, Physics World **14**, 25 (2001).
[2] K. L. Ekinci, Small **1**, 786 (2005).
[3] K. L. Ekinci, X. M. H. Huang, and M. L. Roukes, Applied Physics Letters **84**, 4469 (2004).
[4] R. G. Knobel and A. N. Cleland, Nature **424**, 291 (2003).
[5] M. Li, H. X. Tang, and M. L. Roukes, Nature Publishing Group **2**, 114 (2007).
[6] D. Rugar, R. Budakian, H. J. Mamin, and B. W. Chui, Nature (2004).
[7] M. Blencowe, Physics Reports **395**, 159 (2004).
[8] K. C. Schwab and M. L. Roukes, Physics Today **58**, 36 (2005).
[9] M. D. LaHaye, Science **304**, 74 (2004).
[10] T. Rocheleau, T. Ndukum, C. Macklin, J. B. Hertzberg, A. A. Clerk, and K. C. Schwab, Nature **463**, 72 (2010).
[11] J. D. Teufel, T. Donner, D. Li, J. W. Harlow, M. S. Allman, K. Cicak, A. J. Sirois, J. D. Whittaker, K. W. Lehnert, and R. W. Simmonds, Nature **475**, 359 (2012).
[12] A. H. Safavi-Naeini, J. Chan, J. T. Hill, T. P. M. Alegre, A. Krause, and O. Painter, Physical Review Letters **108**, 033602 (2012).
[13] A. Armour, M. Blencowe, and K. Schwab, Physical Review Letters **88**, 148301 (2002).

[14] J. Sköldberg, T. Löfwander, V. Shumeiko, and M. Fogelström, Physical Review Letters **101**, 087002 (2008).
[15] P. Rabl, P. Cappellaro, M. Dutt, L. Jiang, J. Maze, and M. Lukin, Physical Review B **79**, 041302 (2009).
[16] S. D. Bennett, S. Kolkowitz, Q. P. Unterreithmeier, P. Rabl, A. C. Bleszynski Jayich, J. G. E. Harris, and M. D. Lukin, New Journal of Physics **14**, 125004 (2012).
[17] A. D. O'Connell, M. Hofheinz, M. Ansmann, R. C. Bialczak, M. Lenander, E. Lucero, M. Neeley, D. Sank, H. Wang, M. Weides, J. Wenner, J. M. Martinis, and A. N. Cleland, Nature **464**, 697 (2010).
[18] P. Rabl, S. J. Kolkowitz, F. H. L. Koppens, J. G. E. Harris, P. Zoller, and M. D. Lukin, Nature Physics **6**, 602 (2010).
[19] Z.-L. Xiang, S. Ashhab, J. You, and F. Nori, Reviews of Modern Physics **85**, 623 (2013).
[20] M. Poggio and C. L. Degen, Nanotechnology **21**, 342001 (2010).
[21] H. J. Mamin, M. Poggio, C. L. Degen, and D. Rugar, Nature Publishing Group **2**, 301 (2007).
[22] F. Xue, P. Peddibhotla, M. Montinaro, D. P. Weber, and M. Poggio, Applied Physics Letters **98**, 163103 (2011).
[23] O. Arcizet, V. Jacques, A. Siria, P. Poncharal, P. Vincent, and S. Seidelin, Nature Physics **7**, 879 (2011).
[24] S. Kolkowitz, A. C. Bleszynski Jayich, Q. P. Unterreithmeier, S. D. Bennett, P. Rabl, J. G. E. Harris, and M. D. Lukin, Science **335**, 1603 (2012).
[25] P. Mohanty, G. Zolfagharkhani, S. Kettemann, and P. Fulde, Physical Review B **70**, 195301 (2004).
[26] A. Kovalev, G. Bauer, and A. Brataas, Physical Review B **75**, 014430 (2007).
[27] R. Jaafar, E. Chudnovsky, and D. Garanin, Physical Review B **79**, 104410 (2009).
[28] G. Zolfagharkhani, A. Gaidarzhy, P. Degiovanni, S. Kettemann, P. Fulde, and P. Mohanty, Nature Publishing Group **3**, 720 (2008).
[29] M. Ganzhorn, S. Klyatskaya, M. Ruben, and W. Wernsdorfer, Nature Publishing Group **8**, 165 (2013).
[30] V. Sazonova, Y. Yaish, H. Ustunel, D. Roundy, T. A. Arias, and P. L. McEuen, Nature **431**, 284 (2004).
[31] A. K. Hüttel, G. A. Steele, B. Witkamp, M. Poot, L. P. Kouwenhoven, and H. S. J. van der Zant, Nano Letters **9**, 2547 (2009).
[32] B. Lassagne, Y. Tarakanov, J. Kinaret, D. Garcia-Sanchez, and A. Bachtold, Science **325**, 1107 (2009).
[33] G. A. Steele, A. K. Huttel, B. Witkamp, M. Poot, H. B. Meerwaldt, L. P. Kouwenhoven, and H. S. J. van der Zant, Science **325**, 1103 (2009).
[34] S. Sapmaz, P. Jarillo-Herrero, Y. Blanter, C. Dekker, and H. van der Zant, Physical Review Letters **96**, 026801 (2006).
[35] R. Leturcq, C. Stampfer, K. Inderbitzin, L. Durrer, C. Hierold, E. Mariani, M. G. Schultz, F. von Oppen, and K. Ensslin, Nature Physics **5**, 327 (2009).
[36] J. O. Island, V. Tayari, A. C. McRae, and A. R. Champagne, Nano Letters **12**, 4564 (2012).
[37] E. A. Laird, F. Pei, W. Tang, G. A. Steele, and L. P. Kouwenhoven, Nano Letters **12**, 193 (2012).
[38] P. L. Stiller, S. Kugler, D. R. Schmid, C. Strunk, and A. K. Huttel, physica status solidi (b) **250**, 2518 (2013).
[39] B. J. LeRoy, S. G. Lemay, J. Kong, and C. Dekker, Applied Physics Letters **84**, 4280 (2004).
[40] M. Poot and H. S. J. van der Zant, Physics Reports **511**, 273 (2012).
[41] K. Borysenko, Y. Semenov, K. Kim, and J. Zavada, Physical Review B **77**, 205402 (2008).
[42] F. Kuemmeth, S. Ilani, D. C. Ralph, and P. L. McEuen, Nature **452**, 448 (2008).
[43] T. S. Jespersen, Nature Physics **7**, 348 (2011).
[44] A. Pályi, P. R. Struck, M. Rudner, K. Flensberg, and G. Burkard, Physical Review Letters **108**, 206811 (2012).
[45] C. Ohm, C. Stampfer, J. Splettstoesser, and M. R. Wegewijs, Applied Physics Letters **100**, 143103 (2012).
[46] A. Khaetskii, V. N. Golovach, X. Hu, and I. Žutić, Physical Review Letters **111**, 186601 (2013).
[47] J. Danon, Physical Review B **88**, 075306 (2013).
[48] K. Tsukagoshi, B. W. Alphenaar, and H. Ago, Nature (1999).
[49] A. Cottet, T. Kontos, S. Sahoo, H. T. Man, M.-S. Choi, W. Belzig, C. Bruder, A. F. Morpurgo, and C. Schönenberger, Semiconductor Science and Technology **21**, S78 (2006).
[50] A. Jensen, J. R. Hauptmann, J. Nygård, and P. E. Lindelof, Physical Review B **72**, 035419 (2005).
[51] S. Sahoo, T. Kontos, J. Furer, C. Hoffmann, M. Gräber, A. Cottet, and C. Schönenberger, Nature Physics **1**, 99 (2005).
[52] P. Stadler, W. Belzig, and G. Rastelli, Physical Review Letters **113**, 047201 (2014).
[53] E. A. Laird, F. Kuemmeth, G. Steele, K. Grove-Rasmussen, J. N. rd, K. Flensberg, and L. P. Kouwenhoven, arXiv.org (2014), 1403.6113v1.
[54] M. S. Rudner and E. I. Rashba, Physical Review B **81**, 125426 (2010).
[55] K. Flensberg and C. M. Marcus, Physical Review B **81**, 195418 (2010).
[56] I. Bargatin and M. Roukes, Physical Review Letters **91**, 138302 (2003).
[57] H. Churchill, F. Kuemmeth, J. Harlow, A. Bestwick, E. Rashba, K. Flensberg, C. Stwertka, T. Taychatanapat, S. Watson, and C. Marcus, Physical Review Letters **102**, 166802 (2009).
[58] M. Jonson, Physical Review B (1989).
[59] N. S. Wingreen, K. W. Jacobsen, and J. W. Wilkins, Physical Review B (1989).
[60] K. Flensberg, Physical Review B **68**, 205323 (2003).
[61] S. Braig and K. Flensberg, Physical Review B **68**, 205324 (2003).
[62] A. Mitra, I. Aleiner, and A. Millis, Physical Review B **69**, 245302 (2004).
[63] J. Koch, F. von Oppen, and A. Andreev, Physical Review B **74**, 205438 (2006).
[64] M. Galperin, A. Nitzan, and M. Ratner, Physical Review B **73**, 045314 (2006).
[65] A. Zazunov and T. Martin, Physical Review B **76**, 033417 (2007).
[66] M. Galperin, M. A. Ratner, and A. Nitzan, Journal of Physics: Condensed Matter **19**, 103201 (2007).
[67] R. Egger and A. Gogolin, Physical Review B **77**, 113405 (2008).
[68] O. Entin-Wohlman, Y. Imry, and A. Aharony, Physical Review B **80**, 035417 (2009).
[69] S. Maier, T. L. Schmidt, and A. Komnik, Physical Review B **83**, 085401 (2011).
[70] F. Pistolesi, Journal of Low Temperature Physics **154**, 199 (2009).
[71] F. Cavaliere, E. Mariani, R. Leturcq, C. Stampfer, and M. Sassetti, Physical Review B **81**, 201303 (2010).

[72] D. Braak, Physical Review Letters **107**, 100401 (2011).
[73] F. Haupt, T. Novotný, and W. Belzig, Physical Review B **82**, 165441 (2010).
[74] T. Novotný, F. Haupt, and W. Belzig, Physical Review B **84**, 113107 (2011).
[75] J. Rammer, *Quantum Field Theory of Non-equilibrium States*, 1st ed. (Cambridge University Press, New York, 2007).
[76] J. C. Cuevas and E. Scheer, *Molecular Electronics: An introduction to Theory and Experiment*, 1st ed. (World Scientific Publishing Company, Singapore, 2010).
[77] G. D. Mahan, *Many-Particle Physics*, 3rd ed. (Kluwer Academic/Plenum Publishers, New York, 2000).
[78] H. Bruus and K. Flensberg, *Many-Body Quantum Theory in Condensed Matter Physics: An Introduction*, 1st ed. (Oxford University Press, New York, 2004).
[79] J. Viljas, J. Cuevas, F. Pauly, and M. Häfner, Physical Review B **72**, 245415 (2005).
[80] S. Walter and B. Trauzettel, Physical Review B **83**, 155411 (2011).
[81] G. A. Steele, F. Pei, E. A. Laird, J. M. Jol, H. B. Meerwaldt, and L. P. Kouwenhoven, Nature Communications **4**, 1573 (2013).